Article

Tribological Behavior of Gas-Nitrided 42CrMo4 Steel at Elevated Temperatures

Dominika Panfil-Pryka [1], Michal Kulka [1,*], Mateusz Kotkowiak [1], Jerzy Michalski [2] and Karol Grochalski [3]

1 Institute of Materials Science and Engineering, Poznan University of Technology,
M Sklodowska-Curie Square 5, 60-965 Poznan, Poland; dominika.panfil-pryka@put.poznan.pl (D.P.-P.);
mateusz.kotkowiak@put.poznan.pl (M.K.)
2 Department of Materials Engineering, Czestochowa University of Technology, Armia Krajowa Avenue 19,
42-200 Czestochowa, Poland; jerzymichalski987@gmail.com
3 Institute of Mechanical Technology, Poznan University of Technology, M.Sklodowska-Curie Square 5,
60-965 Poznan, Poland; karol.grochalski@put.poznan.pl
* Correspondence: michal.kulka@put.poznan.pl; Tel.: +48 61 6653575

Abstract: Nitriding is a well-known thermochemical treatment improving the surface hardness and the wear resistance of steel. The phase composition and growth kinetics of the nitrided layer can be controlled using a gas nitriding with changeable nitriding potential. In this work, such a gas nitriding was used to produce, on 42CrMo4 steel, the two nitrided layers differing in the thickness of compound zone and diffusion zone. The microstructure and nanohardness of these layers were studied. For the first time, the tribological behavior of gas nitrided layers at elevated temperatures (from 23 to 400 °C) was investigated. The compound zone consisted of $\varepsilon + (\varepsilon + \gamma')$ iron nitrides and, in the diffusion zone, the nitric sorbite with γ' precipitates was observed. The highest nanohardness was measured in the $\varepsilon + \gamma'$ zone. The lowest values of friction coefficients were obtained if the contact surface of the friction pair entered the $\varepsilon + \gamma'$ zone. After the wear process, at a final temperature of 400 °C, worn surfaces showed only intensive abrasive wear, evidenced by shallow grooves. The increased oxygen content at the edges of wear tracks indicated possible oxidative wear.

Keywords: gas nitriding; compound zone; microstructure; nanohardness; coefficient of friction; wear resistance; elevated temperature

1. Introduction

Gas nitriding is one of the most widely used thermo-chemical surface treatments in various fields of engineering to improve the fatigue strength and wear resistance of machine parts [1–3]. The nitriding process, first developed in the early 20th century, usually produces a diffusion layer rich in nitrogen on the surface of the steel and improves its surface hardness and wear resistance. The nitriding process can be carried out in a solid medium as powder-pack nitriding, in a liquid medium as salt bath nitriding, or in a gaseous medium as conventional, controlled, or low-pressure gas nitriding, as well as plasma (ionic) nitriding under glow-discharge conditions [1]. Among all these nitriding techniques, the controlled gas nitriding [1–7], the low-pressure gas nitriding [8,9] and plasma nitriding [10–12] have the greatest importance.

Low-pressure gas nitriding has recently been intensively developed [8,9]. The main advantage of such nitriding is to accelerate the diffusion of nitrogen into the steel substrate. This process consists of the two stages repeated alternately. During the first stage, the so-called "boost stage", ammonia gas is supplied at a constant low pressure with the flow

rate proportional to the total area of nitrided charge. The second stage, called the "diffusion stage", is carried out in a high vacuum in order to protect the produced nitrided layer against external influences. During this stage, nitrogen diffuses into the steel. Low-pressure gas nitriding has a non-equilibrium nature. Hence, the determination of the nitriding potential and, as a consequence, its control during the process is impossible. Therefore, predicting the effects of the process, i.e., the phase composition of the nitrided layer and its thickness, requires carrying out many tests with various technological parameters (such as temperature, pressure, atmospheric flow rate, and time).

The use of plasma nitriding is very important in the case of materials that are easily passivated, e.g., austenitic steels [11] or titanium alloys [12]. The oxide layers formed on the surface effectively hinder the diffusion of nitrogen into the material. An important feature of plasma nitriding is the ability of the ionized gas to clean the surface of oxides by cathode sputtering. Sometimes this advantage of the plasma process is used before low-temperature gas nitriding in order to activate the surface of austenitic steel [13]. The conventional plasma nitriding often results in a disadvantage, called an "edging effect". This effect can be overcome by decoupling plasma generation from the treated material using an active screen [12]. As in the case of low-temperature process, the nitriding potential cannot be controlled during plasma nitriding.

Many studies have shown that the nitriding process can be used to improve the tribological properties of constructional steels [2–7,14,15], tool steels [16–20], austenitic stainless steels [11,13,21], ferritic–martensitic stainless steels [22], martensitic stainless steels [23,24], or duplex stainless steels [25]. Although the plasma nitriding process has been well developed recently, controlled gas nitriding still predominates in the case of parts with a complicated shape for their homogeneous hardening by diffusion introducing nitrogen.

Controlled gas nitriding enables the control and regulation of the growth of the nitrided layer using the changeable value of the nitriding potential. For the gas nitriding process, it is possible to determine the nitrogen potential and the degree of ammonia dissociation at a specific percentage and flow rate of the atmospheric components [1–7]. The nitriding potential is very important, taking into account the control not only of the growth kinetics of the nitrided layer but the thickness and phase composition of the iron nitrides' zone (the so-called compound zone) [6]. It also guarantees the repeatability of the phase composition at specified nitriding parameters. Usually, the gas nitriding process is carried out at temperatures below 590 °C. As a result of typical gas nitriding, the layer produced generally consists of two zones: a compound zone on the top surface and a diffusion zone beneath it [1]. The compound zone consists of ε iron nitrides ($Fe_{2-3}N$ phase) close to the surface and the mixture of ε and γ' (Fe_4N phase) iron nitrides below. In the diffusion zone, a nitrogen rich solid solution, or nitric sorbite zone with nitride precipitates, is observed [3,6,26]. In general, controlled gas nitriding (at the changeable nitriding potential) allows for obtaining three types of layers: a layer with $\varepsilon + (\varepsilon + \gamma')$ compound zone close to the surface and, with the diffusion zone, a layer with a compound zone containing only γ' nitrides and a nitrided layer composed only of the diffusion zone [3,4,6]. The effect of gas nitriding time on the microstructure and wear resistance of 42CrMo4 steel was studied [27]. The authors reported that gas nitriding advantageously influenced the hardness and adhesive wear resistance of this low alloy steel, both in the case of the nitrided layer with a compound zone and only with a diffusion zone. However, the wear resistance of the layer with the compound zone is better. The microstructure and properties of gas-nitrided of 42CrMo4 steel was also investigated in the paper [28]. The compound zone with ε and γ' nitrides occurred in the nitrided layer, which was characterized by improved hardness, wear resistance, corrosion resistance, and compressive residual stress, as well as by reduced tensile strength or impact strength. In one study [29], the authors

tried to separate the ε and γ′ phases in plasma-nitrided 42CrMo4 steel using color etching techniques. Oberhoffer's reagent was indicated to be the best etchant to separate these two phases.

The compound zone especially improves the tribological properties of a nitrided steel due to its high hardness. However, in some cases, it also reduces the fatigue strength of the layer due to the presence of cracks and pores in this zone [14,30,31]. Simultaneously, the diffusion zone determines the strength of the nitrided layer as well as its fatigue strength [32]. The wear tests of plasma nitrided AISI H11 and H13 tool steels at elevated temperature were reported in one paper [19]. When the temperature of the wear test increased to 200 °C, the friction coefficient was the same as that obtained at room temperature. The wear tests were carried out in air. Therefore, the samples were oxidized. Since the plasma nitrided tool steel samples had a high hardness, the oxide layers formed during the tests protected the samples against the wear and acted as a lubricant. Hence, the lowest values of friction coefficient and volume loss were obtained after the wear tests at 400 °C, indicating the best resistance for wear of the plasma nitrided layers. The best performance at this temperature could be due to the presence of smooth solid compact oxide layers which act as load bearing areas, lowering the contact stress and thus reducing wear. At 600 °C, the samples were more heavily oxidized. This resulted in higher values of the friction coefficient. The increase in the coefficient of friction is attributed to the increased contact area due to the softening of the materials. The wear mechanism was adhesive at room temperature and at 200 °C, whereas it was adhesive and abrasive at more elevated temperature (400 and 600 °C). Similar results were reported after plasma nitriding of AISI H13 steel at different gas mixtures [33].

In general, the abrasive wear could be indicated as the predominant wear mechanism of nitrided steels because of the high surface hardness of nitrided layers and, therefore, less tendency to plastic deformations [34]. Nitriding caused the reduction of the possibility of adhesion between the contacting surfaces by altering the surface structure and reducing the plastic deformation of the specimens' surfaces [15,34]. Usually, the porous ε iron nitrides ($Fe_{2-3}N$ phase) were the reason for the undesirable embrittlement and flaking of the compound zone, and thus, as a consequence, accelerated the destruction and wear of the working parts [6,26]. The investigation of the tribological properties of γ′-Fe_4N phase indicated that it had a lower coefficient of friction than the ε-$Fe_{2-3}N$ phase in a vacuum [35]. However, some papers have reported that the presence of ε iron nitrides in the compound zone after plasma nitriding resulted in better wear and corrosion resistance compared to γ′ iron nitrides (Fe_4N phase), because of its compact close-packed hexagonal structure and higher nitrogen content [16]. The crystallographic orientation was always known as one of the main factors affecting the durability of metallic materials. A drop in the coefficient of friction (CoF) could be found as a result of the easy glide of the planes parallel to the sliding plane. Hence, the particular crystallographic orientation of the (200)γ′ phase was preferred and effective in reducing the plastic deformation during glide. Thus, the single compound zone, composed of only the γ′ phase, was positive for tribological properties, showing the lowest frictional coefficient and lowest wear rate [32]. The gas nitrided samples were characterized by almost the same friction coefficient in a vacuum and in air. Therefore, the gas nitriding did not reduce the friction coefficient in a vacuum [23].

In this work, the microstructure and phase composition of 42CrMo4 steel, after the two different gas nitriding processes, were examined. The nanohardness profiles and, for the first time, the effects of controlled gas nitriding on the tribological behavior at elevated temperature were studied. Microstructure characterization of the gas nitrided layers was described using optical microscopy (OM) and X-ray diffraction (XRD). Nanohardness measurements were performed using a nanoindenter equipped with a Berkovich diamond

tip. The tribological behavior and wear characteristics of the gas nitrided specimens were analyzed using a high-temperature ball-on-disc tribometer. Wear tests were conducted under a constant load of 5 N at different temperatures ranging from room temperature to 400 °C, changing that every 30 min by 100 °C. The aim of this study was to investigate the changes in the tribological performance of nitrided layers after exposure to elevated temperatures and to correlate them with microstructural changes after surface treatment.

2. Materials and Methods

2.1. Material and Controlled Gas Nitriding

The material used in this experiment was 42CrMo4 constructional steel with the following chemical composition: 0.38%–0.45% C, 0.9%–1.2% Cr, 0.4%–0.7% Mn, 0.17%–0.37% Si, 0.15%–0.25% Mo, max 0.3% Ni, max 0.05% V, max 0.2% W, max 0.035% S and max 0.035% P. The specimens were prepared in the form of discs with a diameter of 25.4 mm and a thickness of 6 mm. Then, the samples were austenitized at 860 °C (1123 K), quenched in oil, and then high-temperature tempered at 600 °C (873 K) for 2 h. Such a heat treatment resulted in a sorbite microstructure (a mixture of ferrite and cementite created as a result of the diffusion transformations of martensite) with an average hardness of 270 HV0.05.

The controlled gas nitriding of the samples was carried out in ammonia NH_3 gas at the Institute of Precision Mechanics in Warsaw. The two various processes were carried out in order to produce the compound zones significantly differing in depth. The parameters of these processes are shown in Table 1. During the first process, a temperature of 570 °C (843 K), time of 5 h, and a changeable nitriding potential were used. A second process was performed at a temperature of 580 °C (853 K) for a longer duration of 8 h. The nitriding potential for K_N also changed during this process in order to control the microstructure of the compound zone. This potential is defined by the following equation:

$$K_N = \frac{p_{NH3}}{p_{H2}^{1,5}} \tag{1}$$

where K_N is the nitriding potential ($atm^{-0.5}$), p_{NH3} is the partial pressure of ammonia (atm), and p_{H2} is the partial pressure of hydrogen (atm).

Table 1. Parameters of the controlled gas nitriding.

Nitriding Temperature (°C)	Nitriding Time (h)	Atmosphere	Range of Ammonia Flow Rate (l/min)	Final Nitriding Potential K_N ($atm^{-0.5}$)
570	5	NH_3	1–7	2.52
580	8	NH_3	2–7	3.48

The K_N value was very high in the initial state of both processes: at 570 °C for 5 h and 580 °C for 8 h, being gradually diminished and obtaining its final value of 2.52 and 3.48 $atm^{-0.5}$, respectively. The selection of the appropriate profile of nitriding potential during the process was very important because of its essential influence on the microstructure of compound zone and, in the considered case, its thickness.

2.2. Microstructure Analysis

After the treatment, the specimens were cut perpendicularly to the surface, mounted in a conductive resin, ground, and polished. In order to reveal the microstructure, a typical natal solution was used as an etching reagent. The microstructure of the nitrided samples was observed using a LAB-40 (OPTA-TECH, Poznan, Poland) optical microscope (OM) and MIRA 3 (TESCAN, Poznan, Poland) scanning electron microscope (SEM). The PANalytical

Empyrean X-ray diffractometer (Malvern Panalytical Ltd., Poznan, Poland) with CuK_α radiation was used during the phase analysis of the nitrided layers. Based on the X-ray diffraction (XRD) patterns obtained, the corresponding phases were identified.

2.3. Nanohardness Measurements

The nanohardness profiles vs. the distance from the surface were determined using NHT^2 nanoindenter (Anton Paar, Poznan, Poland) equipped with a Berkovich diamond tip in the shape of regular triangular pyramid. During the tests, the load-displacement curves were recorded representing load vs. penetration depth dependence (Figure 1a). The scheme of the indenter–sample contact during the test is shown in Figure 1b. A maximal load of F_{max} = 50 mN was used. Based on Oliver and Pharr's theory [36], the maximal values of load and penetration depth were equal to F_{max} and h_{max}, respectively. During unloading, the elastic displacements gradually disappeared and, after full removal of the indenter, h_p was assumed as the final depth of the hardness indent.
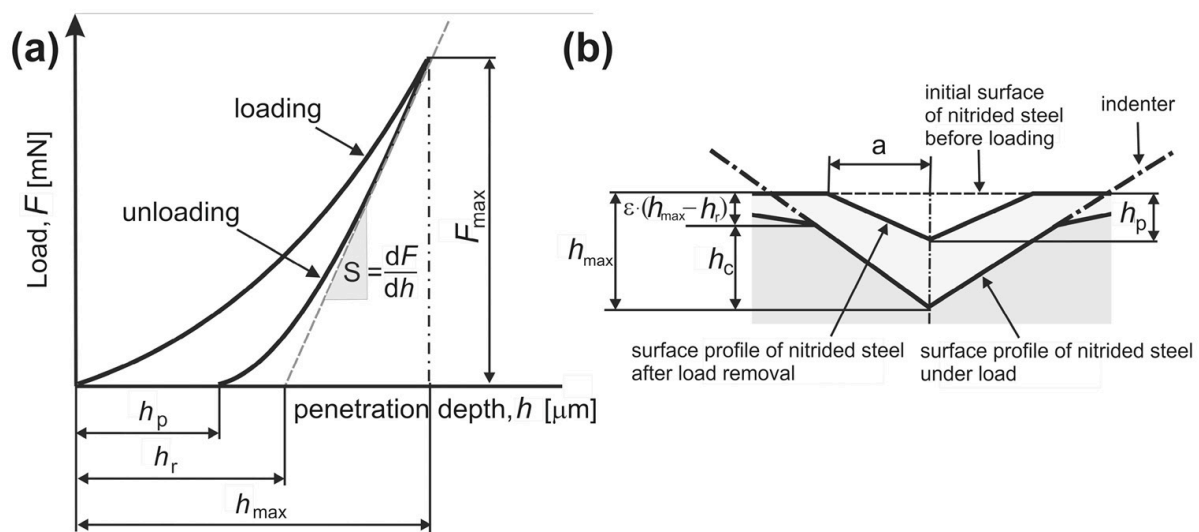
Figure 1. Typical indentation curve (load-displacement curve) (**a**) and schematic representation of the indenter–sample contact (**b**); F_{max}—maximal load; S—contact stiffness; h_p—permanent indentation depth; h_r—tangent indentation depth; h_{max}—maximal indentation depth; h_c—contact depth of the indenter with the sample at F_{max}; ε—geometric constant (0.75 for Berkovich indenter).

Based on the analysis of the curve during loading and unloading, the contact depth h_c was determined. The nanoindentation hardness H_{IT} was defined as an indentation load F_{max} divided by the projected contact area of the indentation A_p according to the equation:

$$H_{IT} = \frac{F_{max}}{A_p}\,(Pa) \tag{2}$$

where H_{IT} is the indentation nanohardness (Pa), F_{max} is the maximal load (N), and A_p is the projected contact area (theoretical or calibrated) (m^2); A_p is a function of contact depth h_c.

In order to determine the Vickers nanohardness, the equation was used as follows:

$$HV_{IT} = \frac{H_{IT}(MPa)}{10.800} \tag{3}$$

where H_{IT} is the indentation nanohardness (MPa), and HV_{IT} is the Vickers nanohardness.

The experimental procedure as well as the calculations applied to determine the values of H_{IT} and HV_{IT} were described in [26] in detail.

2.4. Tribological Properties

"Pin-on-disc" or "ball-on-disc" devices are one of the most common tribometers in the world, used in testing friction and wear of friction pairs with concentrated contact. In this work, the wear tests were performed using a T-21 tribometer (ITE-PIB Radom, Poznan, Poland) and the "ball-on-disc" technique. The scheme of the wear tests is shown in Figure 2. The gas nitrided specimen, made of 42CrMo4 steel disc, was fixed on a rotating shaft, while the Al_2O_3 ball was used as a counter-specimen. The load F_n = 4.9 N (0.5 kgf) was applied, and the rotational speed of the disc specimen was equal to n = 120 min^{-1}. Dry sliding tests were carried out in a special chamber with the possibility of heating. During the tests, the temperature was successively raised from an ambient temperature of 23 °C (296 K) to 100 °C (373 K), 200 °C (473 K), 300 °C (573 K), and 400 °C (673 K). The sample was held at each temperature for 30 min. During the test, the chamber temperature, friction force F_f, and displacement of the contact surface between specimen and counter-specimen were recorded. The friction coefficient was calculated according to the equation:

$$CoF = \frac{F_f}{F_n} \tag{4}$$

where CoF is the coefficient of friction, F_f is the friction force (N), and F_n is the applied load (N).
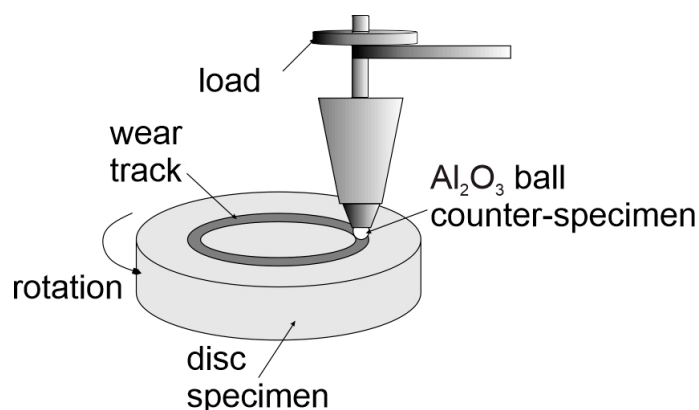

Figure 2. The scheme of the wear test.

The wear tracks were examined using a MIRA 3 (TESCAN, Poznan, Poland) scanning electron microscope (SEM) equipped with an EDS X-ray microanalyzer (Ultim Max 65, Poznan, Poland). The contents of iron, nitrogen, oxygen, and chromium were measured after a wear resistance test. The surface of wear tracks and their depths were determined using a T8000 (Hommel, Poznan, Poland) profilometer.

3. Results and Discussion

3.1. Microstructure Characterization

The scheme of the heat treatment (quenching) and thermochemical treatment (gas nitriding) is shown in Figure 3, with the expected microstructure evolution. After quenching in oil, the microstructure of the 42CrMo4 steel was characterized by the presence of martensite. The high-temperature tempering resulted in obtaining the sorbite in microstructure. The microstructure of the gas-nitrided layers was composed of the $\varepsilon + (\varepsilon + \gamma')$ iron nitrides in the compound zone and with nitric sorbite and γ' precipitates in the diffusion zone. The detailed distribution of nitrogen through the gas-nitrided layer at the nitriding temperature and at ambient temperature after slow cooling was presented in [26].
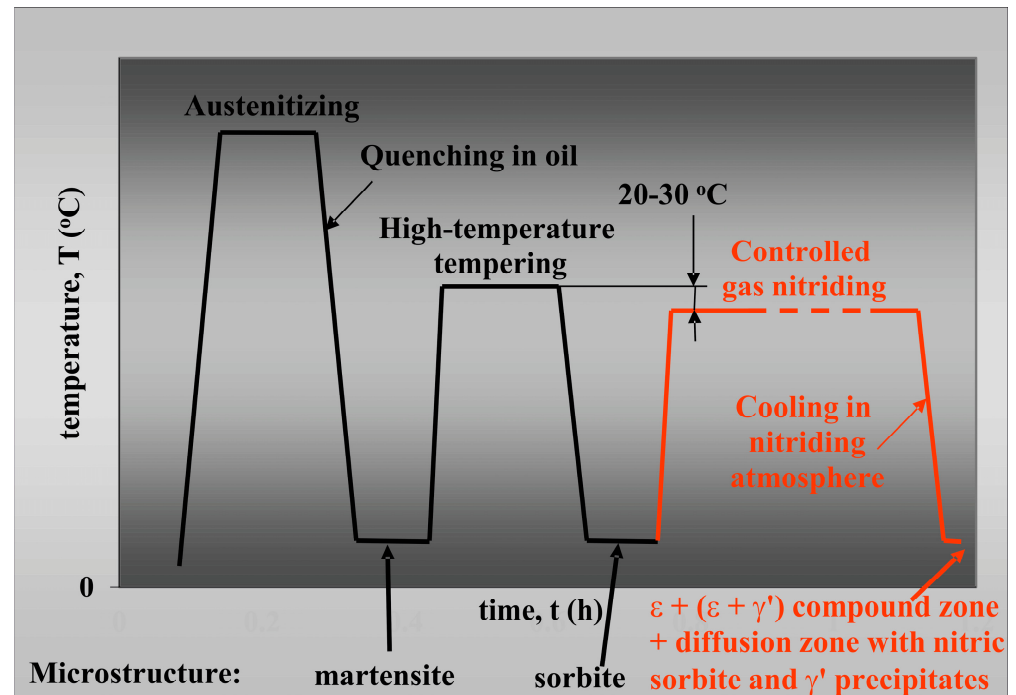
Figure 3. Scheme of the heat treatment (quenching) and thermochemical treatment (gas nitriding) with the expected microstructure evolution.

Figure 4 shows a cross-sectional microstructure of 42CrMo4 steel after the controlled gas nitriding. Before gas nitriding, the substrate material (42CrMo4 steel) was subjected to quenching and high-temperature tempering, i.e., to toughening. After such a heat treatment, the initial microstructure of the base material (before nitriding) consisted of sorbite (a mixture of ferrite and cementite produced as a consequence of the diffusion transformation of martensite). The gas nitrided layers were composed of a surface compound zone and a diffusion zone located below. The interfaces of both the compound zone/diffusion zone and the diffusion zone/substrate were smooth. In the compound zone, the two areas were visible: the region containing the porous ε ($Fe_{2-3}N$) iron nitrides and the region composed of the $\varepsilon + \gamma'$ ($Fe_{2-3}N + Fe_4N$) iron nitrides below the first one. Such a composition in the compound zone resulted from the Fe-N equilibrium diagram as well as the growth kinetics of the nitrided layer; this has been confirmed by many previous studies [1,6,29]. The first process of controlled gas nitriding (carried out at 570 °C for 5 h) resulted in the formation of a thinner compound zone. The average thickness of $\varepsilon + (\varepsilon + \gamma')$ nitrides was about 24.7 µm (Figure 4a). After the second process (at 580 °C for 8 h), the compound zone was significantly thicker, obtaining an average value of 35.9 µm (Figure 4b). Simultaneously, the differences in the thickness of the porous ε zone were visible. The average thickness of this zone was equal to 8.3 µm after the first process and 14.1 µm after the second process. The depth of the diffusion zone was approximately 390 and 580 µm, respectively. This zone was composed of nitric sorbite with precipitates of γ' nitrides.

XRD patterns were obtained using CuK_α radiation. Such radiation is usually characterized by a relatively low penetration depth for metallic materials [37]. It allowed for analyzing a depth up to 20 µm. Such depth did not exceed the thickness of the compound zone in the case of both nitriding processes. Therefore, only the phase composition of the compound zone could be determined. XRD analysis indicated that the compound zone consisted of ε-$Fe_{2-3}N$ and γ'-Fe_4N phases after the first gas nitriding process (at 570 °C for 5 h), as shown in Figure 5a. XRD patterns obtained after the second process (at 580 °C for 8 h), indicated that the compound zone was also composed of ε-$Fe_{2-3}N$ and γ'-Fe_4N

phases (Figure 5b). However, the ε iron nitrides predominated in this case, and only small amounts of low-intensity peaks originating from γ′ phase were observed. The reason for this was the relatively thick zone with ε iron nitrides (14.1 μm).
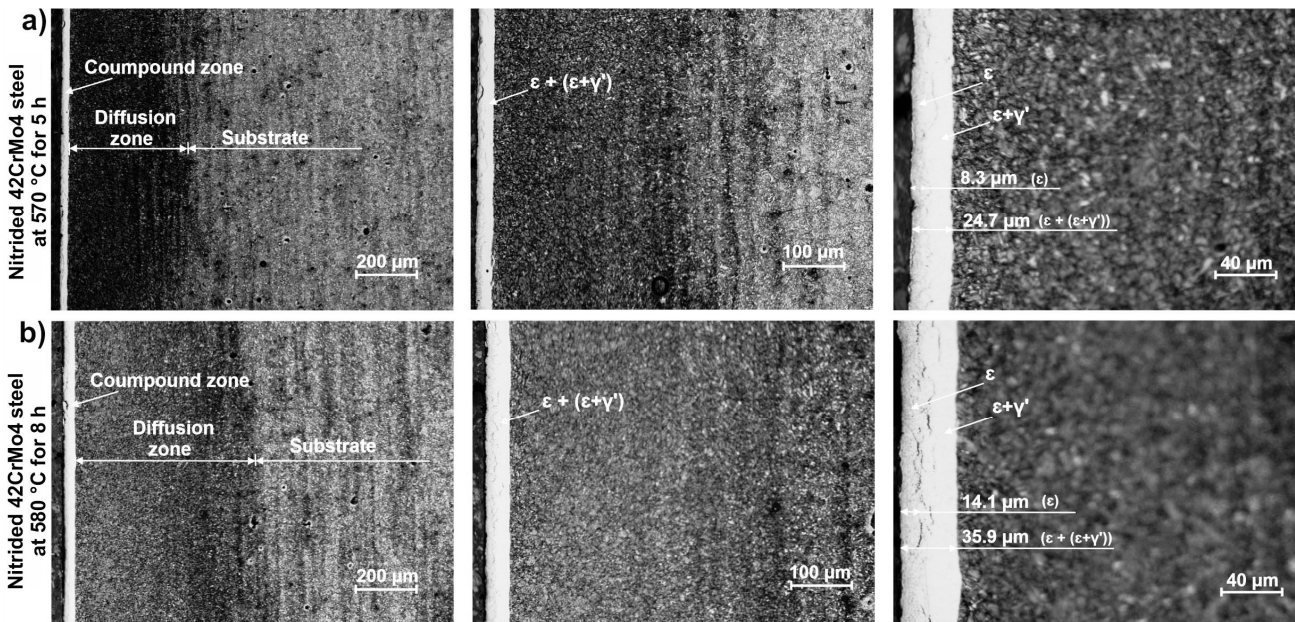

Figure 4. OM images of the gas-nitrided layer produced on 42CrMo4 steel: (**a**) at 570 °C for 5 h and (**b**) at 580 °C for 8 h.
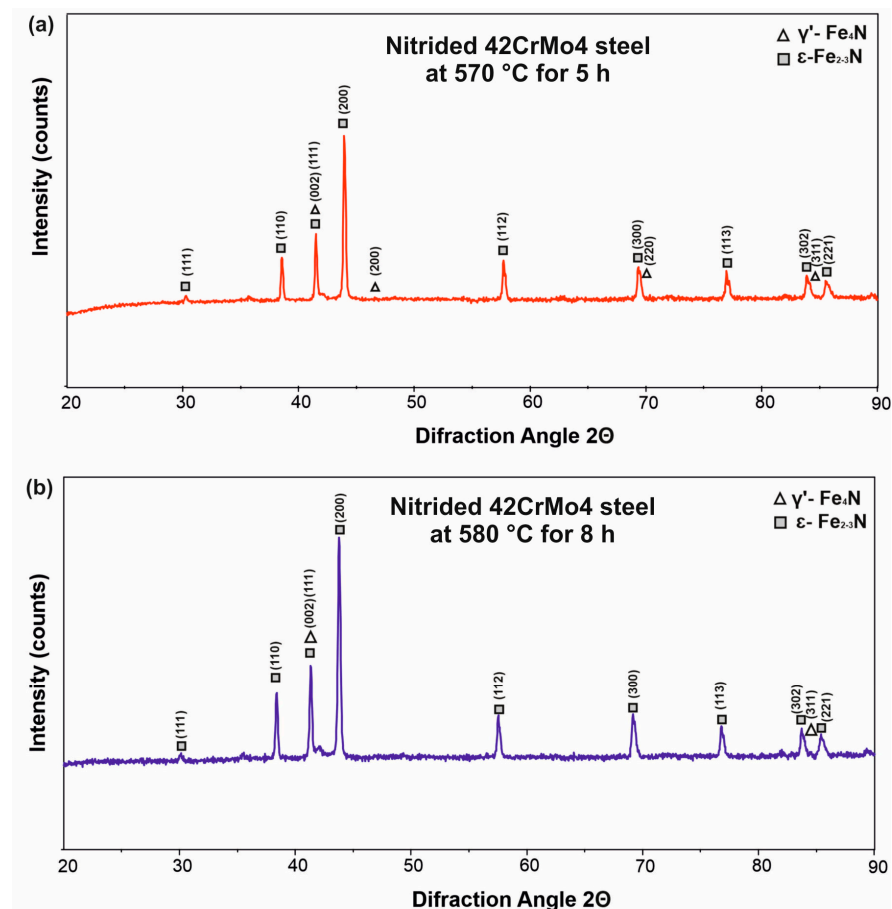

Figure 5. X-ray diffraction patterns of the gas-nitrided layer produced on 42CrMo4 steel: (**a**) at 570 °C for 5 h and (**b**) at 580 °C for 8 h.

3.2. Nanohardness Profiles

The nanohardness profiles along the cross-section of the gas nitrided specimens were measured vs. the distance from the surface with a nanohardness tester on polished metallographic specimens. These profiles are depicted in Figure 6. The measurements were performed on the etched specimens so that it was easy to identify the zones occurring in the surface layer, as well as the indents in these zones. The Vickers hardness HV_{IT} was calculated based on the measurements of indentation hardness H_{IT} according to Equation (2). The nanohardness differed in the compound zone depending on its phase composition. Lower values of hardness were observed in the porous ε iron nitrides when compared to the $\varepsilon + \gamma'$ zone. It was characteristic for both nitriding processes that the lowest hardness was measured close to the surface (in the ε zone). The hardness values in the ε zone increased when the distance from the surface increased from 501 to 724 HV_{IT} in the case of the first process (nitriding at 570 °C for 5 h), and from 708 to 785 HV_{IT} in the nitrided layer produced at 580 °C for 8 h. Whereas the $\varepsilon + \gamma'$ zone was characterized by a significantly higher Vickers hardness HV_{IT}. The measured values ranged in this zone of the layer from 975 to 1005 HV_{IT} and from 996 to 1183 HV_{IT} for the processes carried out at 570 °C for 5 h and at 580°C for 8 h, respectively. Next, below the compound zone, hardness gradually diminished in the diffusion zone from 609 HV_{IT} below the iron nitrides to 390 HV_{IT} at the end of this zone and from 720.3 to 346.5 HV_{IT}, respectively, in the case of the nitriding processes at 570 °C for 5 h, and at 580 °C for 8 h, respectively. The averaging Vickers hardness of the substrate with sorbite microstructure was 374 and 345 HV_{IT}, respectively. Quite large hardness fluctuations in the diffusion zone and slightly smaller ones in the substrate were caused by the relatively low load used during measurements (50 mN). This resulted in small indents that could hit different phases in the diffusion zones (nitric sorbite or γ' precipitates) differing significantly in hardness. The ranges of hardness values measured in all the zones of nitrided layers in relation to the depth of specific zones are shown in Table 2.
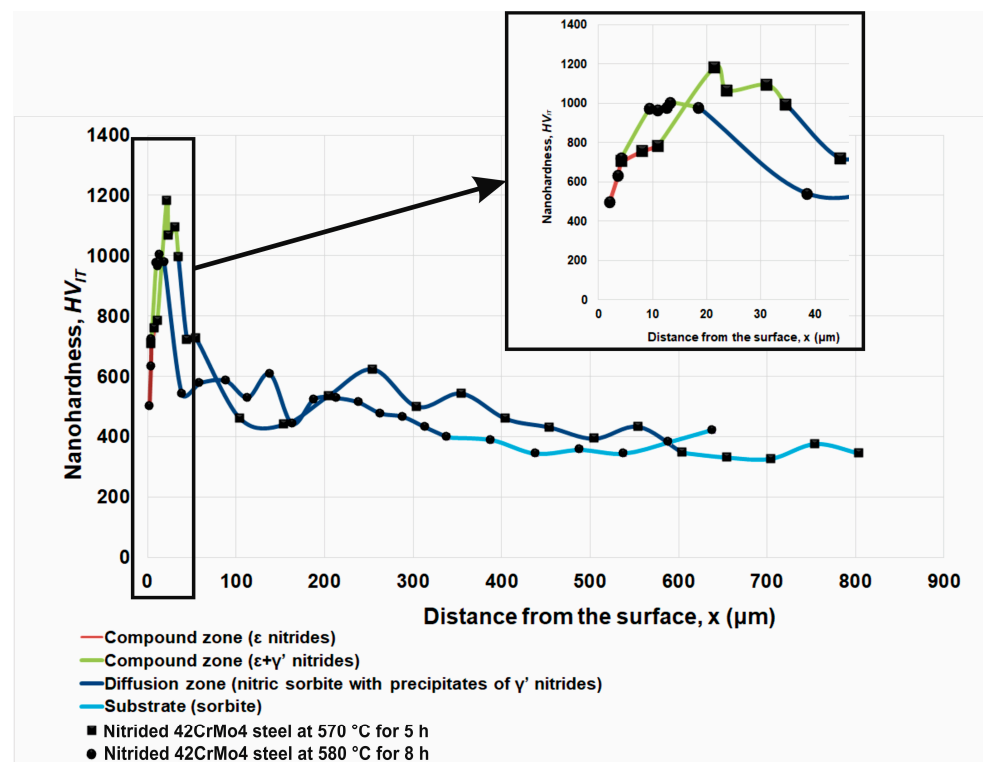

**Figure 6.** Nanohardness HV_{IT} vs. depth of the gas nitrided layers produced on the 42CrMo4 steel.

Table 2. Ranges of HV_{IT} values in all the zones of gas nitrided layers.

Type of the Layer	Zone of Measurements	Average Depth of the Zone (μm)	Hardness Range HV_{IT}
Nitrided layer produced at 570 °C for 5 h	ε	8.3	501–724
	$\varepsilon + \gamma'$	24.7	965–1005
	Diffusion zone	~390 *	390–609
	Substrate	-	345–422
Nitrided layer produced at 580 °C for 8h	ε	14.1	708–785
	$\varepsilon + \gamma'$	35.9	996–1183
	Diffusion zone	~580 *	382–720
	Substrate	-	327–376

* measured to the point where the hardness corresponded to the hardness of the substrate.

3.3. Tribological Behavior

The temperature during the wear test was recorded and changed every 30 min from room temperature (23 °C) to 400 °C. The results of the temperature measurements are shown in Figure 7 for nitrided layers produced both at 570 °C for 5 h (Figure 7a) and at 580 °C for 8 h (Figure 7b). In the initial stage of heating, the working chamber and temperature fluctuations were visible. The largest temperature fluctuations were observed at a nominal temperature of 100 °C. Wear tests conducted at a nominal temperature of 200 °C were characterized by slightly smaller fluctuations, and at 300 and 400 °C the temperature was already well stabilized.
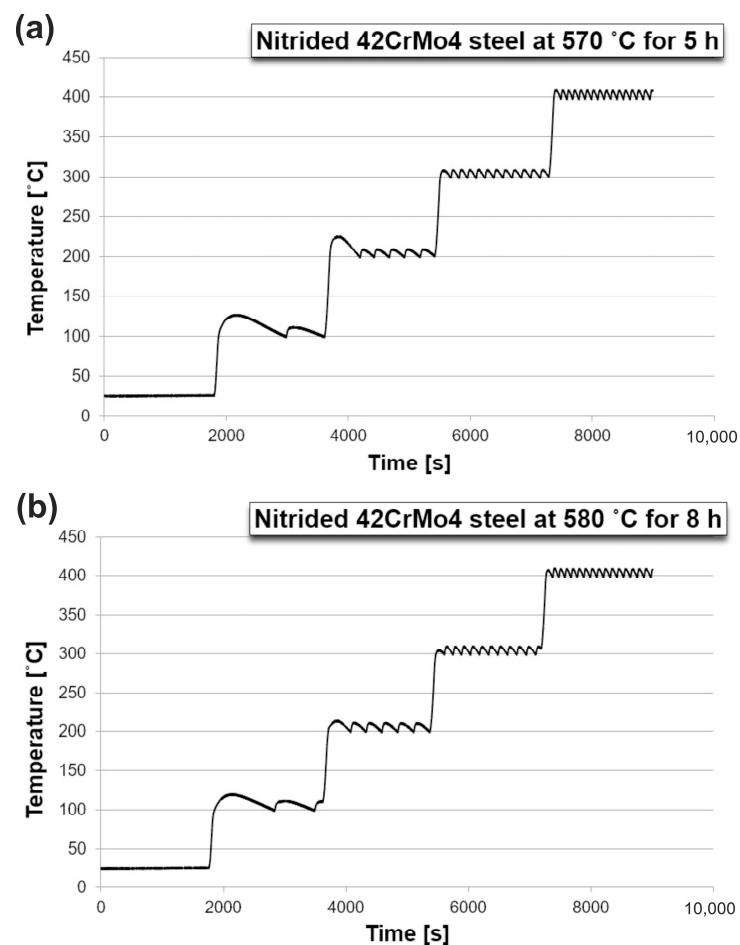
Figure 7. Changes in the temperature of the working chamber during the wear tests of nitrided 42CrMo4 steel: (**a**) at 570 °C for 5 h and (**b**) at 580 °C for 8 h.

Wear tests were carried out continuously at a temperature increased every half hour on both nitrided layers produced at 570 °C for 5 h and at 580 °C for 8 h. During the tests, the friction force F_f was recorded, enabling the calculation of coefficient of friction (*CoF*) at known load F_n (50 mN). The course of changes in the friction coefficient during tests of both nitrided layers is shown in Figure 8. The wear tests started at room temperature (23 °C). The first stage of wear consisted in grinding-in and lasted for approximately 460 s for the nitrided layer formed at 570 °C for 5 h (Figure 8a) and for 400 s for the second nitrided layer (Figure 8b). The wear behavior of both nitrided layers differed during the test. After grinding-in, the CoF value of the layer produced at 570 °C for 5 h, still increased at room temperature obtaining the average value of 0.73. The temperature elevated to 100 °C caused initial decrease in the CoF to values characteristic of the end of the grinding-in stage. Next, the friction coefficient still increased quickly. Finally, the average CoF value at 100 °C was equal to 0.93. At a temperature of 200 °C, the friction coefficient initially continued to increase rapidly, and then its value slowly began to decrease. However, its average value during this stage was as high as 1.14. A value of the friction coefficient exceeding 1 could indicate high adhesion of the friction pair (nitrided sample—Al_2O_3 ball), which could lead to adhesive wear and the formation of adhesion craters. However, this was difficult to observe during the continuous wear test. Elevating the temperature of the wear chamber to 300 °C caused the friction coefficient to steadily decrease and its average value dropped to 0.90. The lowest average CoF value (0.69) was calculated at the test temperature of 400 °C. At this temperature, the friction coefficient gradually decreased (Figure 8a).
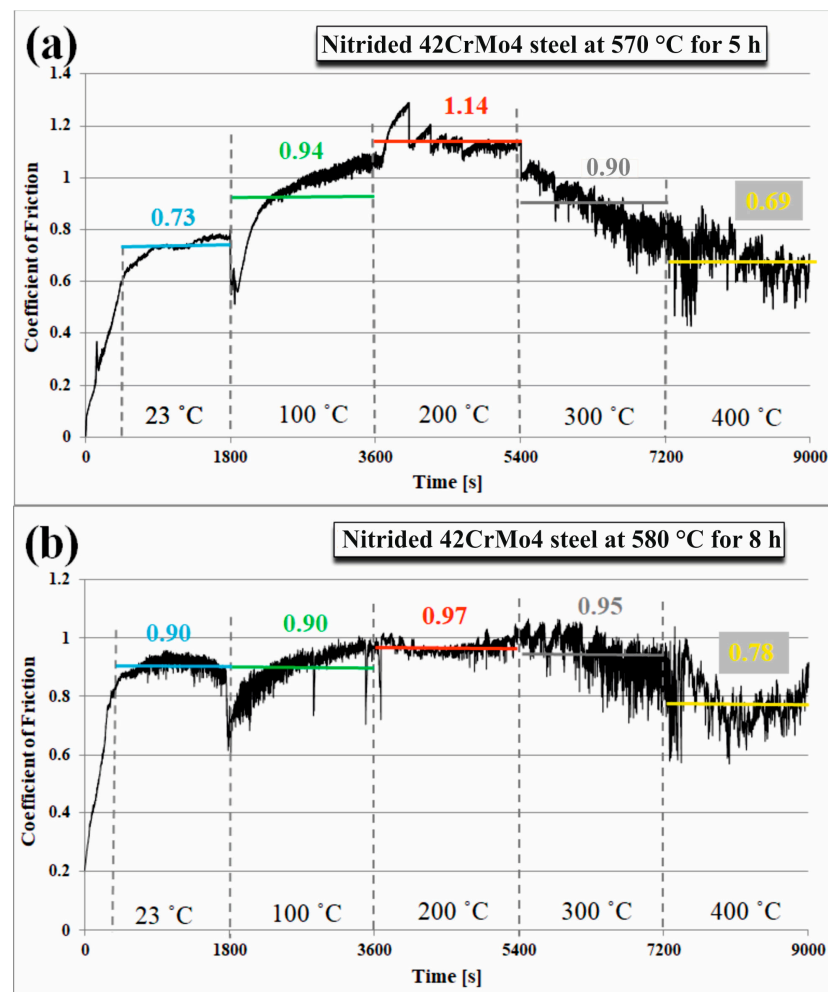
Figure 8. Friction coefficients vs. time of friction at elevated temperatures for the gas nitrided layer produced: (**a**) at 570 °C for 5 h and (**b**) at 580 °C for 8 h.

In the case of the nitrided layer produced at 580 °C for 8 h (Figure 8b), after the grinding-in stage at an ambient temperature (23 °C), the friction coefficient first increased and then decreased to the value before the end of grinding-in, reaching an average value of 0.90. Increasing the temperature of the working chamber to 100 °C resulted in a gradual increase in the friction coefficient to a value close to 1, and its average value was also 0.90. At a temperature of 200 °C, the CoF was characterized by slight fluctuations in its value, but its average value was the highest and amounted to 0.97. At the beginning of the friction wear process, at a temperature of 300 °C, the friction coefficient exceeded 1, which could result in adhesive wear that was difficult to observe. Then, a gradual decrease in the CoF value was noted, which resulted in its average value of 0.95. The final temperature of the wear test (400 °C) was characterized by an initial decrease and then an increase in the friction coefficient. Its average value at this temperature was the lowest and amounted to 0.78.

After the wear tests, the specimens with a nitrided layer produced both at 570 °C for 5 h and at 580 °C for 8 h were cut perpendicularly to their surface and perpendicularly to the wear scars formed during the test on the specimen surface. In this way, it was possible to observe the cross-section of the samples at the final contact point with the counter-sample using an optical microscope. OM images of wear tracks are shown in Figure 9.
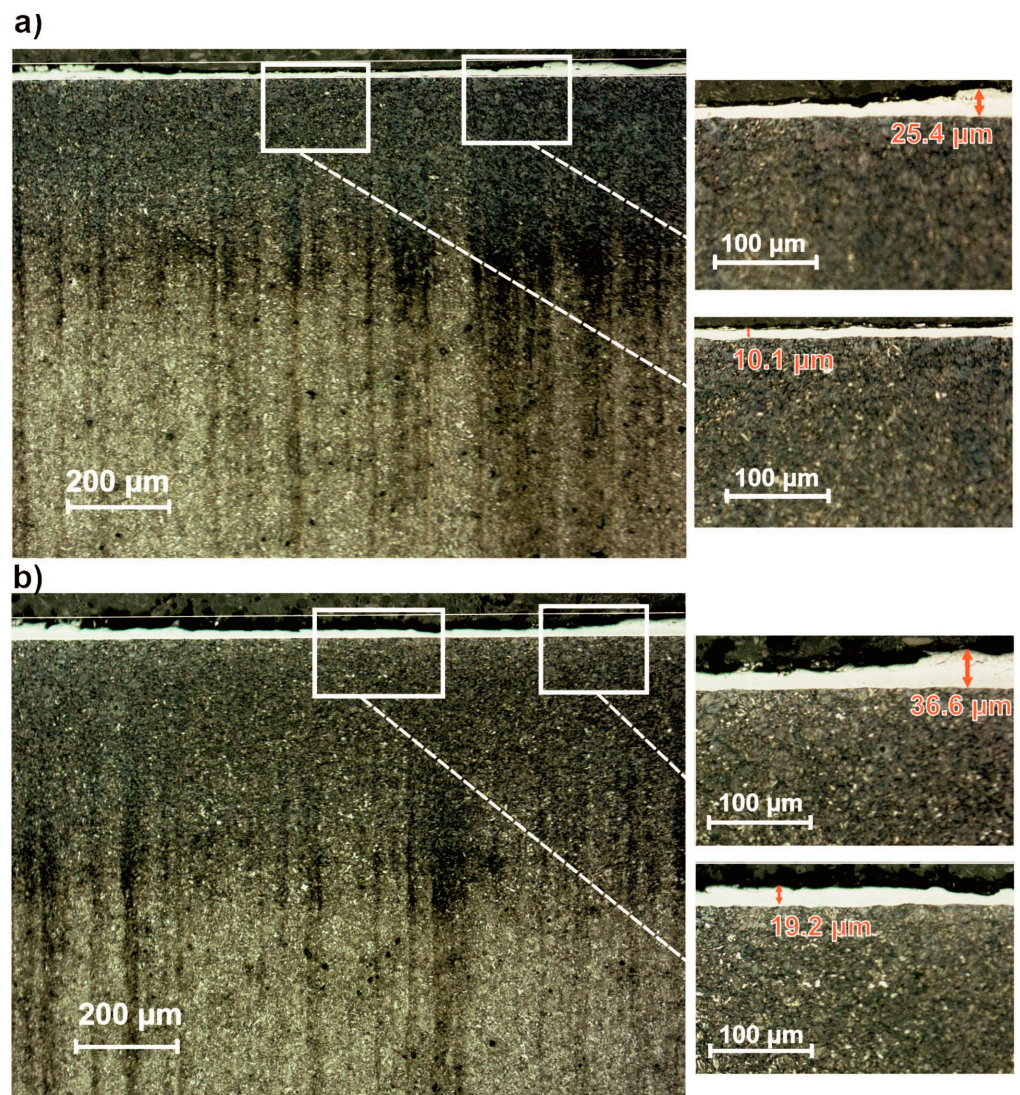

Figure 9. OM images of the specimens at the final contact point with counter-specimen: (**a**) specimen nitrided at 570 °C for 5 h, (**b**) specimen nitrided at 580 °C for 8 h.

Based on these images, the depths of the wear tracks could be calculated (see Figure 9). The measurements indicated that the initial thickness of $\varepsilon + (\varepsilon + \gamma')$ was equal to 25.4 μm for the layer produced at 570 °C for 5 h and 36.6 μm in the case of specimen nitrided at 580 °C for 8 h. After the wear tests, the remaining compound zone was 10.1 mm and 19.2 mm thick, respectively (Figure 9). This means that the final depth of the wear track corresponded to 15.3 and 17.4 μm in the considered cases.

To more precisely determine the depth and width of the wear tracks for the tested specimens and counter-specimens mating with them, a Hommel T8000 profilometer was used, enabling contact measurements of the geometric structure of the surface. The results are presented in Figure 10 for a specimen nitrided at 570 °C for 5 h and Al_2O_3 counter-specimen. Figure 10a,b show 3D views of the specimen and counter-specimen, respectively. Using 2D profiles of the specimen and counter-specimen surfaces (Figure 10c,d), it was possible to determine the depths of the wear tracks. The depth of the wear track for the nitrided specimen was equal to 14.5 μm, corresponding well to the value of 15.3 μm measured using the OM image (Figure 9a). In the case of the counter-specimen the depth of wear track amounted to 8.86 μm.
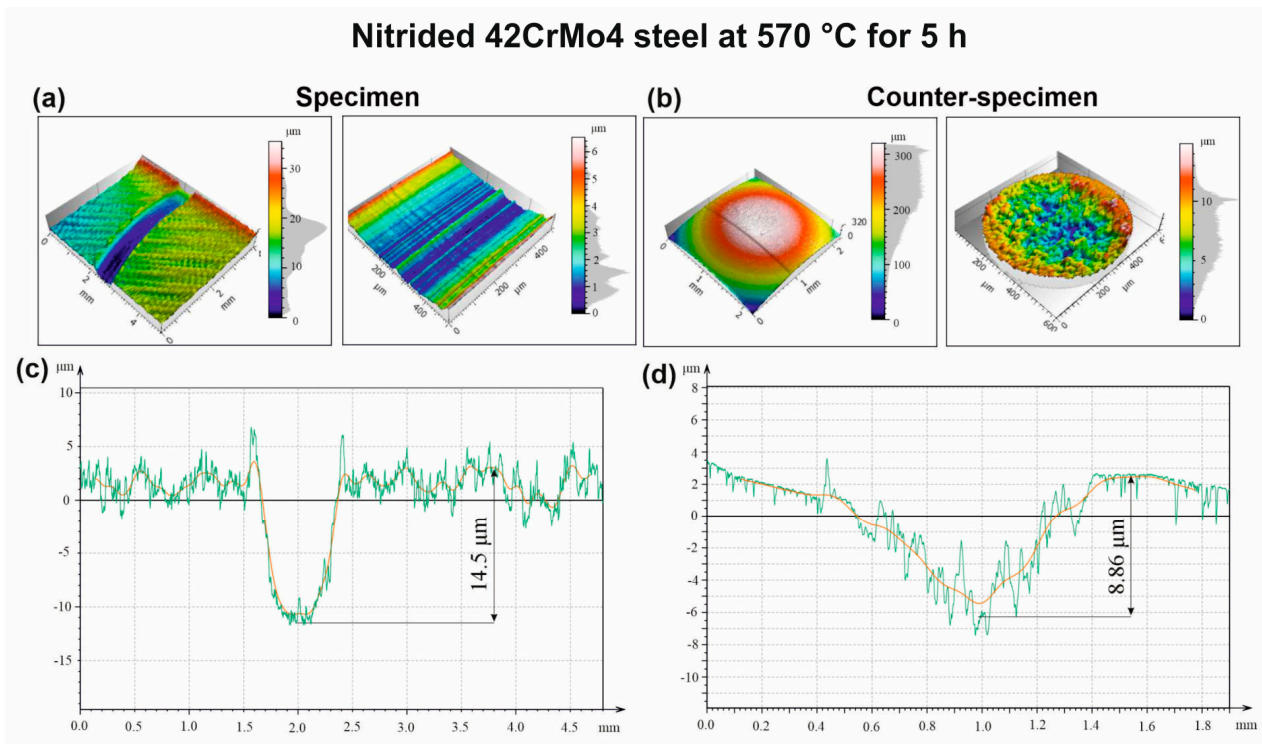
Figure 10. Surface topography of the wear track remaining in the gas nitrided layer produced at 570 °C for 5 h and in the counter-specimen made by the Al_2O_3 ball: (**a**) 3D surface view of the specimen; (**b**) 3D surface view of the counter-specimen; (**c**) 2D profile of the specimen; (**d**) 2D profile of the counter-specimen.

Figure 11 shows the surface topography of the worn nitrided layer produced at 580 °C for 8 h mating it with the counter-specimen. A 3D surface view of nitrided specimen and counter-specimen is visible in Figure 10a,b, respectively. A 2D surface profile (Figure 11c,d) made it possible to determine the depth of the wear tracks, which were 15.1 μm and 11.2 μm for the sample and counter-sample, respectively. Such a depth of the wear track in the nitrided specimen was only slightly lower than that (17.4 μm) determined based on the OM image (Figure 9b).
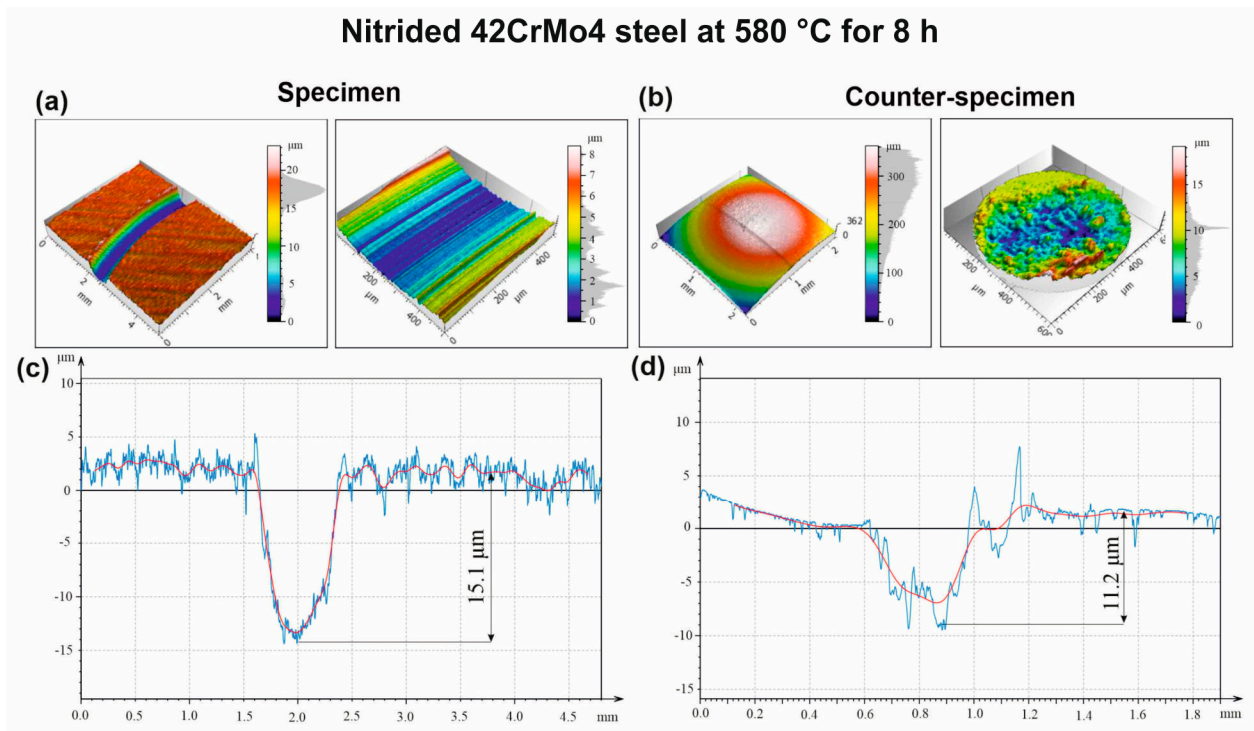
Figure 11. Surface topography of wear track remaining in the gas nitrided layer produced at 580 °C for 8 h and in the counter-specimen made by the Al_2O_3 ball: (**a**) 3D surface view of the specimen; (**b**) 3D surface view of the counter-specimen; (**c**) 2D profile of the specimen; (**d**) 2D profile of the counter-specimen.

The hardness of the nitrided layer produced at 580 °C for 8 h seemed to be higher, but only when the measurements reach the compounds zone with the composition of $\varepsilon + \gamma'$, i.e., at the depth of more than 15 µm (see the enlarged part of Figure 6). For the layer produced at 570 °C for 5 h, the thickness of porous ε zone was lower, hence the hardest $\varepsilon + \gamma'$ zone appeared at the lower depth. This is the reason that the depth of wear track was larger for the nitrided layer produced at 580 °C for 8 h.

Based on these more accurate measurements of the depths of the wear tracks in gas nitrided layers and measurements of the displacement of the contact surface between specimen and counter-specimen, it was possible to determine the predicted depths of the wear tracks in the nitrided layers during continuous wear at elevated temperatures. During the wear tests, the displacement of the contact surface between the specimen and counter-specimen was recorded. However, it was difficult to determine the depth of the wear track based on these measurements because of the changeable temperature and different thermal expansion coefficients of the sample and counter-sample. Therefore, to predict the depth of the wear tracks during tests at various temperatures, an actual measurement with a profilometer after the final stage of the wear test at a temperature of 400 °C was used. In this way, a graph of the predicted wear track depth throughout the test was prepared, as shown in Figure 12.

It was observed that in the case of both nitrided layers, each subsequent wear test temperature results in a greater increase in the depth of the wear track. In the case of the nitrided layer produced at 570 °C for 5 h (Figure 12a), these increments of the wear track depth ranged from 0.24 µm at room temperature (23 °C) to 5.31 µm at 400 °C. Whereas the increment of the wear track depth in the nitrided layer produced at 580 °C for 8 h (Figure 12b) increased from 0.17 µm at 23 °C to 5.98 µm at 400 °C. This analysis made it possible to predict how the position of the sample and counter-sample contact changed during a continuous wear test in which the temperature of the working chamber was

changed step-by-step, obtaining individual average values of the friction coefficient. Table 3 shows the CoF values, the predicted depths of wear tracks, and the phase compositions of the gas nitrided layers tested at various temperatures.
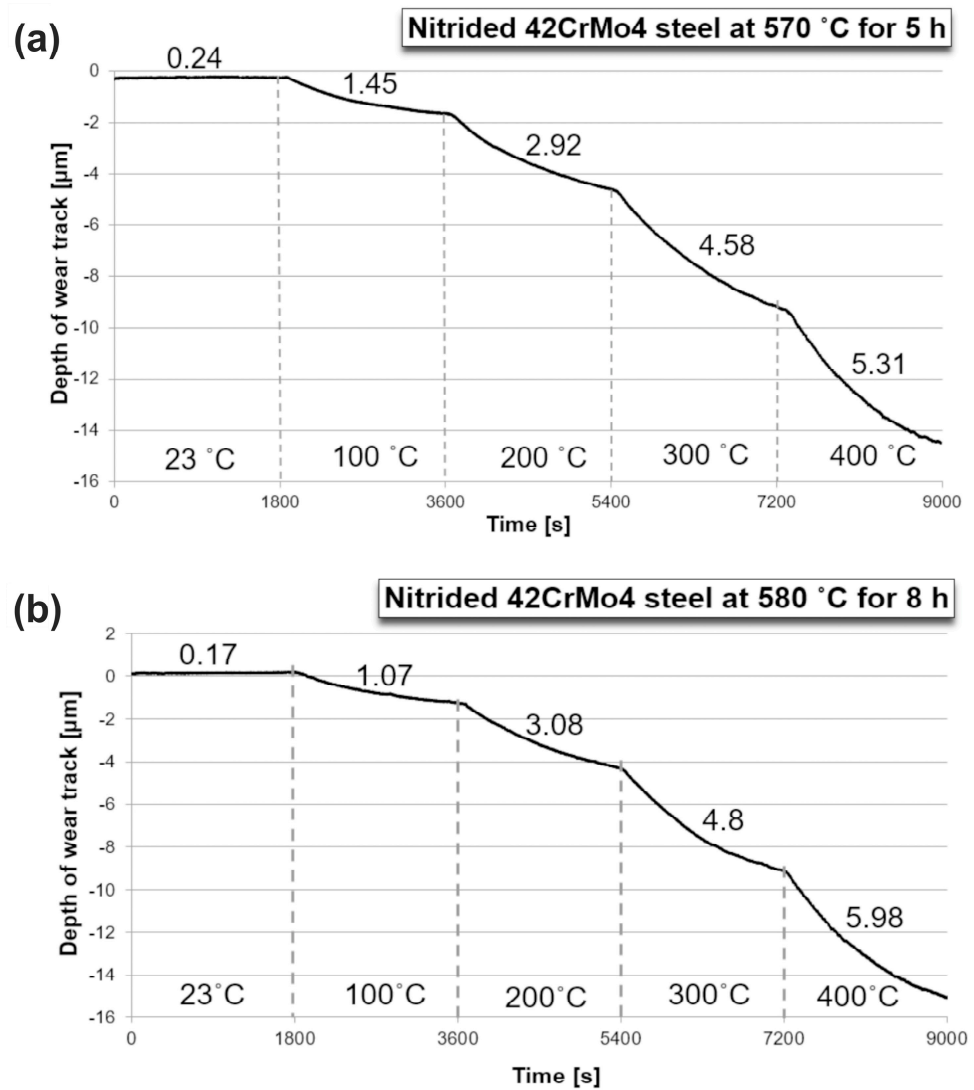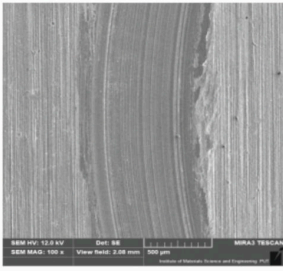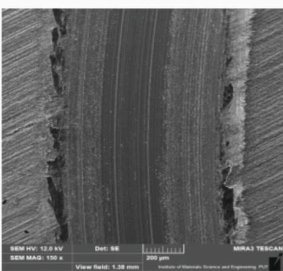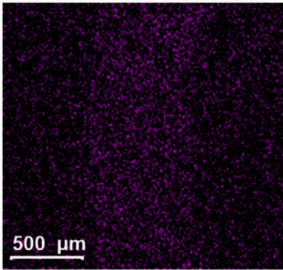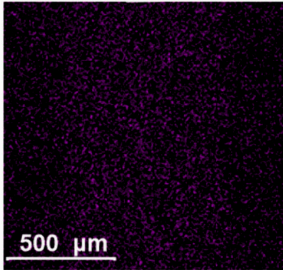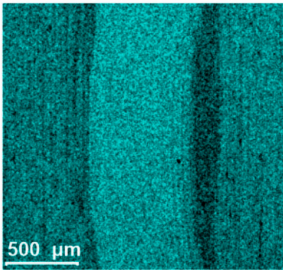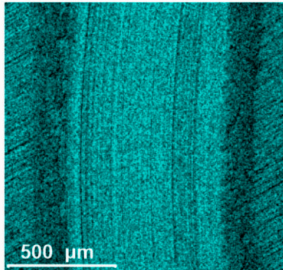

Figure 12. Predicted depth of the wear track vs. time of friction in the gas nitrided layers produced: (**a**) at 570 °C for 5 h and (**b**) at 580 °C for 8 h.

Table 3. The average coefficients of friction predicted depths of wear tracks, and corresponding phase composition.

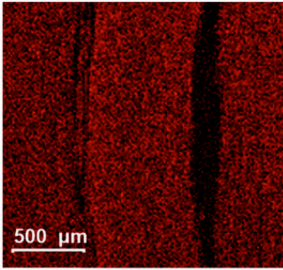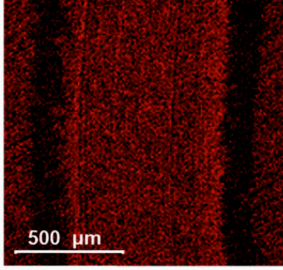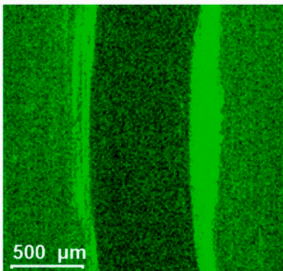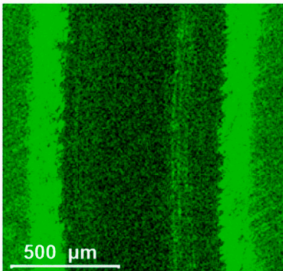| -		Nitrided Layer Produced at 570 °C for 5 h			Nitrided Layer Produced at 580 °C for 8 h		
Temperature of Working Chamber (°C)	Average Coefficient of Friction	Predicted Depth of Wear Track (µm)	Phase Composition of the Layer	Average Coefficient of Friction	Predicted Depth of Wear Track (µm)	Phase Composition of the Layer
23	0.73	0.24	ε	0.90	0.17	ε
100	0.94	1.69	ε	0.90	1.24	ε
200	1.14	4.61	ε	0.97	4.32	ε
300	0.90	9.91	$\varepsilon + \gamma'$	0.95	9.12	ε
400	0.69	14.5	$\varepsilon + \gamma'$	0.78	15.1	$\varepsilon + \gamma'$

The average values of friction coefficients were relatively high if the wear by friction proceeded in the ε-Fe$_{2\text{-}3}$N phase. The wear of the gas nitrided layer produced at 570 °C for 5 h proceeded exclusively in this phase up to 200 °C (Table 3), and the average CoF value increased from 0.73 at 23 °C to an extremely high value of 1.14 at 200 °C. Such a high coefficient of friction could result from the high adhesion of the specimen with the ε phase and counter-specimen in the area of their contact surface. If so, the adhesive craters should be visible on the worn surface of the nitrided specimen. However, the wear test was continuously carried out, and there was no possibility to confirm such a wear mechanism. After the test at 300 °C the position of the contact surface of the friction pair, corresponding to the predicted depth of the wear track (9.91 µm), exceeded the thickness of ε-Fe$_{2\text{-}3}$N phase, i.e., 8.3 µm (Figure 4). Hence, the wear by friction partially proceeded in the $\varepsilon + \gamma'$ zone (Table 3). Taking into account that this zone was more compact, porosity-free and, according to the literature data, more wear-resistant, a decrease in the friction coefficient was expected. And, indeed, the average CoF value was lower at 300 °C and amounted to 0.90. Further wear process at a temperature of 400 °C resulted in another reduction of the friction coefficient to 0.68 due to the increasing percentage of the $\varepsilon + \gamma'$ zone on the contact surface of the sample and counter-sample. For the nitrided layer produced at 580 °C for 8 h, its wear proceeded exclusively in the ε-Fe$_{2\text{-}3}$N phase up to 300 °C (Table 3). The average friction coefficients were high, reaching the values of 0.90, 0.90, 0.97, and 0.95, for temperatures of 23 °C, 100 °C, 200 °C, and 300 °C, respectively. Only during friction at a temperature of 400 °C did the position of the contact surface of the friction pair exceeded the boundary between the ε and $\varepsilon + \gamma'$ zones. This resulted in a significant reduction in the average CoF value to 0.79. Also, in this case, the friction coefficient reached values higher than 1 during the wear test at temperatures of 200 and 300 °C. Unfortunately, the continuous wear process with sudden changes in temperature made it impossible to observe the worn surface in order to identify the effects of adhesive wear. To summarize, the final decrease in the coefficient of friction was caused by the presence of ε-Fe$_3$N + γ'-Fe$_4$N iron nitrides, which increased the durability of the machine parts and tools due to high wear resistance [19,20]. The single phase γ' in the compound zone was still more beneficial to tribological properties, showing the lowest frictional coefficient and lowest wear rate [29].

SEM images of the worn surfaces after the high-temperature wear tests of gas nitrided layers (at 570 °C for 5 h and at 580 °C for 8 h) are shown in Figure 13. The observed worn surfaces showed primarily the intensive abrasive wear, assuming the shape of shallow grooves. There were no signs of severe plastic deformation as well as no signs of adhesive wear evidenced by adhesion craters. The EDS pattern of selected elements (Figure 13) on worn surfaces showed the significant content of iron and nitrogen, i.e., elements creating the ε or γ' iron nitrides. Additionally, the increased content of oxygen was observed, especially at the edges of the wear tracks. This could indicate possible oxidative wear. Such a wear mechanism could also have a positive effect on the friction coefficient, reducing it at the end of the test. However, it could also be the result of the oxidation of particles detached from the surface of the sample or counter-sample during abrasion. Such a combination of abrasive and oxidative wear has often been reported in the literature [37], as has the combination of abrasive, adhesive, and oxidative wear [38,39], which could occur during intermediate test stages at high CoF values. In the future, it would be necessary to investigate the tribological behavior of the produced nitrided layers separately at each of the wear temperatures used in this work.

Figure 13. SEM images of worn surfaces of the gas nitrided layers and EDS patterns of elements characteristic of the gas-nitrided specimens (Fe, N, Cr) and oxygen after the high-temperature wear test with the change in the temperature every 30 min with a final temperature of 400 °C.

4. Summary and Conclusions

Controlled gas nitriding in ammonia gas was used in order to produce the two different nitrided layers on 42CrMo4 steel. The aim of this study was to evaluate and compare the tribological behavior of these layers at elevated temperatures. Therefore, the nitrided specimens were subjected to continuous wear tests with sudden changes in temperature every 30 min from a room temperature of 23 to 400 °C. Based on a detailed analysis of the obtained results, the following conclusions could be formulated:

The microstructure of both gas nitrided layers consisted of the compound zone with $\varepsilon + (\varepsilon + \gamma')$ iron nitrides close to the surface and diffusion zone with nitric sorbite and γ' precipitates. The main differences between both layers concerned the thickness of the compound zone and the total thickness of the layer (including the diffusion zone).

The nitrided layer produced at 570 °C for 5 h was characterized by the average total thickness of the compound zone of 24.7 μm (including the ε zone with a thickness of 8.3 μm) and a total thickness of 390 μm, whereas the second layer produced at 580 °C for 8 h had a thicker compound zone of 35.9 mm (including the ε zone with a thickness of 14.1 μm) as well as a thicker total layer (590 μm).

The highest nanohardness of both nitrided layers was measured in the $\varepsilon + \gamma'$ zone. The nanohardness of ε iron nitrides was significantly lower, probably because of the porosity of this zone. In the diffusion zone, the nanohardness gradually diminished to the values characteristic of the toughened substrate.

The wear on the gas nitrided layer with a thinner compound zone (produced at 570 °C for 5 h) proceeded exclusively in the ε-$Fe_{2-3}N$ phase up to 200 °C, and the average friction coefficient increased from 0.73 at room temperature (23 °C) to 1.14 at 200 °C. The friction coefficient values started to decrease from the moment the contact surface of the friction pair entered the $\varepsilon + \gamma'$ zone. This zone is characterized by improved wear resistance compared to ε nitrides. Hence, the average value of the CoF diminished to 0.90 at 300 °C and to 0.69 at 400 °C.

In the case of the gas nitrided layer with a thicker compound zone (produced at 580 °C for 8 h), the wear proceeded exclusively in the ε-$Fe_{2-3}N$ phase up to 300 °C, obtaining the average friction coefficients of 0.90, 0.90, 0.97, and 0.95 at room temperature (23 °C), at 100 °C, at 200 °C, and at 300 °C, respectively. At 400 °C, the friction coefficient values started to decrease as a result of entering the contact surface of the friction pair into the $\varepsilon + \gamma'$ zone. Hence, the average value of the CoF diminished to 0.78 at 300 °C and to 0.69 at 400 °C.

During the wear carried out in phase ε, the values of the friction coefficients often exceeded the value of 1, which indicated high adhesion of the sample and counter-sample and could result in adhesive wear. However, the continuous wear process at elevated temperatures made it impossible to observe the effects of such a wear mechanism.

After the wear process at a final temperature of 400 °C, worn surfaces showed the intensive abrasive wear, assuming the shape of shallow grooves. There were no signs of severe plastic deformation as well as no signs of adhesive wear. The increased oxygen content at the edges of the wear tracks could indicate possible oxidative wear, positively influencing the friction coefficient.

Author Contributions: Conceptualization, D.P.-P. and M.K. (Michal Kulka); methodology, D.P.-P. and M.K. (Michal Kulka); validation, D.P.-P. and M.K. (Michal Kulka); formal analysis, D.P.-P. and M.K. (Michal Kulka); investigation, D.P.-P., M.K. (Michal Kulka), M.K. (Mateusz Kotkowiak), J.M., and K.G.; resources, D.P.-P. and M.K. (Michal Kulka); data curation, D.P.-P. and M.K. (Michal Kulka); writing—original draft preparation, D.P.-P. and M.K. (Michal Kulka); writing—review and editing, D.P.-P. and M.K. (Michal Kulka); visualization, D.P.-P. and M.K. (Michal Kulka); supervision, D.P.-P. and M.K. (Michal Kulka); project administration, D.P.-P.; funding acquisition, D.P.-P. All authors have read and agreed to the published version of the manuscript.

Institutional Review Board Statement: Not applicable.

Informed Consent Statement: Not applicable.

Data Availability Statement: The authors confirm that the data supporting the findings of this study are available within the article.

Conflicts of Interest: The authors declare no conflicts of interest.

References

1. Mittemeijer, E.J. Fundamentals of nitriding and nitrocarburizing. In *ASM Handbook: Steel Heat Treating Fundamentals and Processes*; Dossett, J., Totten, G.E., Eds.; 4A, ASM International: Materials Park, OH, USA, 2013; pp. 619–646.
2. Małdziński, L.; Tacikowski, J. ZeroFlow gas nitriding of steels. In *Thermochemical Surface Engineering of Steels Improving Materials Performance*; Mittemeijer, E.J., Somers, M.A.J., Eds.; Woodhead Publishing Series in Metals and Surface Engineering: Number 62; Elsevier: Amsterdam, The Netherlands, 2015; pp. 459–483.
3. Michalski, J.; Wach, P.; Tacikowski, J.; Betiuk, M.; Burdynski, K.; Kowalski, S.; Nakonieczny, A. Contemporary Industrial Application of Nitriding and Its Modifications. *Mater. Manuf. Process.* **2009**, *24*, 855–858. [CrossRef]
4. Michalski, J.; Tacikowski, J.; Wach, P.; Lunarska, E.; Baum, H. Formation of single-phase layer of γ′-nitride in controlled gas nitriding. *Met. Sci. Heat Treat.* **2005**, *47*, 516–519. [CrossRef]
5. Frączek, T.; Prusak, R.; Michalski, J.; Kowalewska-Groszkowska, M. Kinetics of Iron Nitride Layer Growth during the Nitriding of AISI 1085 Non-Alloy Steel and AISI 52100 Alloy Steel. *Materials* **2024**, *17*, 4623. [CrossRef] [PubMed]
6. Michalski, J.; Tacikowski, J.; Wach, P.; Ratajski, J. Controlled gas nitriding of 40 HM and 38 HMJ steel grades with and without the surface compound layer, composed of iron nitrides. *Maint. Probl.* **2006**, *2*, 43–52.
7. Frączek, T.; Prusak, R.; Michalski, J.; Skuza, Z.; Ogórek, M. The Influence of Selected Process Parameters on the Efficiency of the Process of Gas Nitriding of AISI 1085 Steel. *Materials* **2024**, *17*, 2600. [CrossRef]
8. Kula, P.E.; Wołowiec, E.; Pietrasik, R.; Dybowski, K.; Januszewicz, B. Non-steady state approach to the vacuum nitriding for tools. *Vacuum* **2013**, *88*, 1–7. [CrossRef]
9. Wołowiec-Korecka, E.; Michalski, J.; Januszewicz, B. The Stability of the Layer Nitrided in Low-Pressure Nitriding Process. *Coatings* **2023**, *13*, 257. [CrossRef]
10. Roliński, E. Plasma-assisted nitriding and nitrocarburizing of steel and other ferrous alloys. In *Thermochemical Surface Engi-neering of Steels Improving Materials Performance*; Mittemeijer, E.J., Somers, M.A.J., Eds.; Woodhead Publishing Series in Metals and Surface Engineering: Number 62; Elsevier: Amsterdam, The Netherlands, 2015; pp. 413–457.
11. Frączek, T.; Prusak, R.; Ogórek, M.; Skuza, Z. Nitriding of 316L Steel in a Glow Discharge Plasma. *Materials* **2022**, *15*, 3081. [CrossRef]
12. Frączek, T.; Prusak, R.; Ogórek, M.; Skuza, Z. The Effectiveness of Active Screen Method in Ion Nitriding Grade 5 Titanium Alloy. *Materials* **2021**, *14*, 3951. [CrossRef]
13. Baranowska, J.; Franklin, S.E.; Pelletier, C.G.N. Tribological behavior and mechanical properties of low temperature gas ni-trided austenitic steel in relation to layer morphology. *Wear* **2005**, *259*, 432–438. [CrossRef]
14. Kikuchi, S.; Komotori, J. Evaluation of the Gas Nitriding of Fine Grained AISI 4135 Steel Treated with Fine Particle Peening and Its Effect on the Tribological Properties. *Mater. Trans.* **2015**, *56*, 556–562. [CrossRef]
15. Zhong, H.; Dai, L.; Yue, Y.; Wang, B.; Zhang, X.; Tan, C.; Ma, M.; Liu, R. Tribological properties of plasma-nitrided AISI 4340 steel in vacuum. *Mater. Sci. Technol.* **2016**, *32*, 275–281. [CrossRef]
16. Mashreghi, A.R.; Soleimani, S.M.Y.; Saberifar, S. The investigation of wear and corrosion behavior of plasma nitrided DIN 1.2210 cold work tool steel. *Mater. Des.* **2013**, *46*, 532–538. [CrossRef]
17. Miyamto, J.; Abraha, P. The effect of plasma nitriding treatment time on the tribological properties of the AISI H13 tool steel. *Surf. Coat. Technol.* **2019**, *375*, 15–21. [CrossRef]
18. Almeida, E.A.D.S.D.; Milan, J.C.G.; Da Costa, C.E. Acquired Properties Comparison of Solid Nitriding, Gas Nitriding and Plasma Nitriding in Tool Steels. *Mater. Res.* **2015**, *18*, 27–35. [CrossRef]
19. Kumar, A.; Kaur, M.; Singh, S.; Joseph, A.; Jhala, G.; Bhandari, S. High-temperature tribological studies of plasma-nitrided tool steels. *Surf. Eng.* **2018**, *34*, 620–633. [CrossRef]

20.	Wen, Z.; Dejun, K. Surface characteristics and hight-temperature wear of plasma intruded layer on steel H13. *Met. Sci. Heat Treat.* **2020**, *61*, 717–723. [CrossRef]

21.	Lin, N.; Liu, Q.; Zou, J.; Guo, J.; Li, D.; Yuan, S.; Ma, Y.; Wang, Z.; Wang, Z.; Tang, B. Surface Texturing-Plasma Nitriding Duplex Treatment for Improving Tribological Performance of AISI 316 Stainless Steel. *Materials* **2016**, *9*, 875. [CrossRef]

22.	Umemura, M.; Varela, L.; Pinedo, C.; Cozza, R.; Tschiptschin, A.; Umemura, M.; Varela, L.; Pinedo, C.; Cozza, R.; Tschiptschin, A. Assessment of tribological properties of plasma nitrided 410S ferritic-martensitic stainless steels. *Wear* **2019**, *426-427*, 49–58. [CrossRef]

23.	Yang, J.; Liu, Y.; Ye, Z.; Yang, D.; He, S. Microstructure and tribological characteristics of nitrided layer on 2Cr13 steel in air and vacuum. *Surf. Coatings Technol.* **2009**, *204*, 705–712. [CrossRef]

24.	Li, Y.; Zhang, S.-Z.; Qiu, J.-X.; Xiu, J.-J.; Ye, Q.-W.; Liu, Z.-L. Effects of electric properties on microstructure, corrosion and wear characteristic of the nitride layer preparation on 2Cr13 stainless steel by plasma nitriding. *Acta Metall. Sin.* **2019**, *32*, 733–745. [CrossRef]

25.	Zhao, S.; Wang, L. Formation and properties of nitrided layer on 2205 duplex stainless steel by anodic plasma-nitriding assisted with hollow cathode discharge. *J. Mater. Res. Technol.* **2024**, *31*, 3652–3660. [CrossRef]

26.	Panfil, D.; Kulka, M.; Wach, P.; Michalski, J.; Przestacki, D. Nanomechanical properties of iron nitrides produced on 42CrMo4 steel by controlled gas nitriding and laser heat treatment. *J. Alloy. Compd.* **2017**, *706*, 63–75. [CrossRef]

27.	Terres, M.A.; Ammari, L.; Chérif, A. Study of the Effect of Gas Nitriding Time on Microstructure and Wear Resistance of 42CrMo4 Steel. *Mater. Sci. Appl.* **2017**, *08*, 493–507. [CrossRef]

28.	Wu, W.; Sun, G. On Industrial Gas Nitriding of 42CrMo Steels for Tie Bars of Two Platen Injection Molding Machines. *J. Mater. Eng. Perform.* **2024**, 1–16. [CrossRef]

29.	Kovács, D.; Szabó, A. The separation of ε- and γ'-phases in the plasma nitrided layer by colour etching techniques. *Metall. Res. Technol.* **2021**, *118*, 315. [CrossRef]

30.	Schwarz, B.; Göhring, H.; Meka, S.R.; Schacherl, R.E.; Mittemeijer, E.J. Pore Formation Upon Nitriding Iron and Iron-Based Alloys: The Role of Alloying Elements and Grain Boundaries. *Met. Mater. Trans. A* **2014**, *45*, 6173–6186. [CrossRef]

31.	Varanasi, R.S.; Koyama, M.; Yokoi, M.; Ootani, Y.; Kubo, M.; Tanahara, K.; Umezawa, O. Understanding crack growth within the γ' Fe4N layer in a nitrided low carbon steel during monotonic and cyclic tensile testing. *J. Mater. Sci.* **2024**, *59*, 14639–14652. [CrossRef]

32.	Wang, Y.-Z.; Yan, M.-F.; Chen, Z.-B.; Zhang, C.-S.; You, Y. Crystallographic texture evolution of γ'-Fe4N and its influence on tribological properties of nitrided steel. *Acta Metall. Sin.* **2018**, *31*, 371–379. [CrossRef]

33.	Kumar, A.; Kaur, M.; Joseph, A.; Jhala, G.; Nanda, T.; Singh, S. High-Temperature Wear and Frictional Performance of Plasma-Nitrided AISI H13 Die Steel. *Lubricants* **2023**, *11*, 448. [CrossRef]

34.	Dayanç, A.; Karaca, B.; Kumruoğlu, L. Improvement of Tribological Properties of Steel Camshaft by Plasma Nitriding. *Acta Phys. Pol. A* **2019**, *135*, 786–792. [CrossRef]

35.	Yang, J.; Liu, Y.; Ye, Z.; Yang, D.; He, S. Microstructural and tribological characterization of plasma- and gas-nitrided 2Cr13 steel in vacuum. *Mater. Des.* **2011**, *32*, 808–814. [CrossRef]

36.	Oliver, W.C.; Pharr, G.M. An improved technique for determining hardness and elastic modulus using load and displacement sensing indentation experiments. *J. Mater. Res.* **1992**, *7*, 1564–1583. [CrossRef]

37.	Hirsch, T.; Hoffmann, F.; Mayr, P. Röontgenographische untersuchungen mikrostruktureller kenngr€oßen von verbindungss-chichten gasnitrierter stähle, Härterei-Technische Mitteilungen. *HTM J. Heat Treat. Mater.* **1996**, *51*, 390–398. [CrossRef]

38.	Ralls, A.M.; Leong, K.; Liu, S.; Wang, X.; Jiang, Y.; Menezes, P.L. Unraveling the friction and wear mechanisms of surface nanostructured stainless-steel. *Wear* **2023**, *538–539*, 205185. [CrossRef]

39.	Zhang, Y.; Hou, W.; Yu, J.; Chen, C.; Zhou, L. The Role of Carbon in Wear Resistance of CoCrFeNiTi0.5 High-Entropy Alloy Layer. *J. Mater. Eng. Perform.* **2024**, 1–13. [CrossRef]